The Mechanical Performance of a Liao Dynasty Five-Step Outer Eave Column-Head Dougong Bracket: A Numerical Investigation

Chang Chen,^a Yuanhe Li,^{a,*} Dongnan Han,^a Hongfa Kang,^a Jibin Wang,^b Lijun Liu,^c Lei Pang,^c and Wenyu Cao ^d

The Dougong bracket is a critical seismic-resistant element in traditional Chinese timber structures, yet its complex mechanical behavior requires further investigation. This study numerically evaluated the static structural performance of a Liao Dynasty 'Five-Step Outer Eave Column-Head Dougong Bracket' from the Dule Temple Gate using finite element analysis. An orthotropic constitutive model calibrated with Pinus sylvestris test data and the Hill yield criterion were implemented in ANSYS. Simulations under vertical monotonic and horizontal low-cycle reversed loads assessed strength, deformation, and energy dissipation. Key findings include a maximum vertical load-bearing capacity of 344 kN, with stress concentrations up to 27.4 MPa at the Huagong-Ludou interface. Horizontal loading revealed symmetrical hysteresis loops, peak loads of 999 kN (Y-axis) and 522 kN (X-axis), ductility coefficients of 2.45 to 3.63, and equivalent viscous damping values of 0.097 to 0.122. The vertical response exhibited tri-linear stiffness degradation, while horizontal behavior followed multi-linear restoring force models. These results validate FEA as an efficient tool for assessing Dougong brackets, supporting the conservation and understanding of historical timber structures.

DOI: 10.15376/biores.21.1.221-236

Keywords: Numerical simulation; Quasi-static response; Seismic performance; Historical timber structures; Pinus sylvestris

Contact information: a: School of Architecture and Art Design, Inner Mongolia University of Science & Technology, Baotou 014010, P.R. China; b: Zhongche Times Electric Drive Co., Ltd., Zhuzhou 412000, P.R. China; c: Inner Mongolia Zhongyu Aerospace Engineering Planning and Design Co., Ltd., Baotou 014010, P.R. China; d: Beijing Zhongbang Huijie Engineering Consulting Co., Ltd., Hohhot 010010, P.R. China; *Corresponding author: 121868212@qq.com Chang Chen and Yuanhe Li contributed equally to this work.

INTRODUCTION

The Dule Temple Gate (Fig. 1), located in Jizhou District, Tianjin, China, is a National Priority Protected Cultural Heritage site. The Liao Dynasty (907 to 1125 CE) was a Khitan-led imperial regime in East Asia, contemporaneous with the Song Dynasty to its south. Its territory spanned much of modern-day northern China, Mongolia, and parts of the Russian Far East, forming a multicultural empire that blended nomadic traditions with Chinese administrative practices. As patrons of Buddhism, the Liao rulers commissioned numerous temple complexes, whose architecture reflects both ethnic Khitan characteristics and influences from Tang and Song building traditions. The Dule Temple Gate, as one of the extremely rare surviving Liao monastic buildings, offers invaluable evidence of this

dynastic legacy. Constructed in 984 CE during the Liao Dynasty, it stands as one of only three extant Liao-era monastic structures. Sicheng Liang, a pioneering architectural historian, acclaimed its significance: "This structure inherits the architectural legacy of the Tang Dynasty while pioneering Song-style construction techniques, serving as a critical resource for studying the evolution of Chinese architectural styles and a rare architectural treasure". The Dougong, a quintessential structural component in ancient Chinese timber architecture, functions as a transitional system between columns and roof structures. Functionally, the Dougong system serves to extend eave projections, decrease span lengths of beams, and redirect roof loads downward to vertical structural elements via its interconnected bracket assemblies (Deng et al. 2023; Song et al. 2023; Liu et al. 2025). Structurally, the Dougong is organized by a tier-based framework, where each "jump" defined as a horizontal projection originating from the Ludou (base block)—introduces an additional overlapping layer. Each jump may consist of arch arms (huagong) or cantilevered ang elements, each contributing a distinct structural increment. Historical precedents include up to five successive jumps, maintaining structural integrity in accordance with traditional proportional rules (Fig. 2). The terminology follows a conventional formula: one jump indicates a four-tier system, two jumps correspond to five tiers, three to six tiers, four to seven, and five jumps to eight tiers. Hence, the overall number of tiers is derived by adding three to the number of jumps. Illustrating this system, the outer eave column-head Dougong at the Dule Temple Gate represents a five-tier arrangement, achieved through two jumps from the base block—a characteristic indicative of Liao Dynasty architectural tradition.



Fig. 1. The Dule Temple Gate





Fig. 2. The authentic Five-tier outer eave column-head Dougong bracket in the Dule Temple Gate

Following the modular system prescribed in *Yingzao Fashi* (Treatise on Architectural Methods, Song Dynasty), Dougong brackets are classified into eight grades based on dimensional hierarchies, each with distinct scale factors tailored to buildings of varying magnitudes (Xue *et al.* 2016; Wu *et al.* 2018; Sha *et al.* 2021). In accordance with *Yingzao Fashi* (Song Dynasty architectural treatise), the Dougong bracket examined in this study corresponds to the third-grade timber within the cai-fen modular system (Chen *et al.* 2025). As stipulated in the treatise, one fen° unit for the third-grade timber is defined as 15.5 mm. The research studied the outer eave column-head Dougong of Dule Temple Gate, comprising 38 modular units—24 primary members and 14 wooden pins—categorized into load-bearing and connective types. Figures 3 and 4 illustrate the test model's perspective view and exploded assembly diagram, delineating its hierarchical composition.



Fig. 3. The perspective view of 'Five-tier Outer Eave Column-head Dougong Bracket' test model of the Dule Temple Gate



Fig. 4. The exploded assembly diagram of 'Five-tier Outer Eave Column-head Dougong Bracket' test model of the Dule Temple Gate

The experimental investigation of traditional timber structures faces significant economic challenges, particularly in constructing full-scale Dougong bracket models, which require substantial material and labor investments (Chen *et al.* 2018; Meng *et al.* 2019). Conventional mechanical testing methodologies, dependent on instrumented measurement points, are inherently limited by systematic errors and spatial resolution constraints, compromising data reliability in complex structural systems. In contrast, finite element analysis (FEA) has emerged as a robust computational tool for characterizing Dougong mechanics, validated through three decades of methodological refinement and empirical verification (Wu *et al.* 2020; Wang *et al.* 2022; Sha *et al.* 2024). This paradigm shift offers dual advantages: 1) elimination of physical specimen fabrication costs, and 2) precise control over boundary conditions and material anisotropy, enabling targeted analysis of critical structural interfaces (Sciomenta *et al.* 2018).

These indices characterize strength, deformation, and energy dissipation. Strength characteristics include the ultimate bearing capacity and stress distribution patterns. Deformation mechanisms cover stiffness degradation and displacement gradients. Energy dissipation is assessed through hysteretic energy absorption and equivalent viscous damping. Through systematic simulation of vertical (Z-axis) monotonic and horizontal (X/Y-axis) low-cycle loading protocols, this study establishes a validated numerical approach for heritage timber structure assessment. The methodology demonstrates a high level of correlation with physical test data while significantly reducing experimental costs, offering an efficient approach for analyzing historical construction techniques and supporting conservation strategies.

EXPERIMENTAL

Numerical Simulation

The finite element analysis was conducted using an orthotropic constitutive model calibrated with the mechanical properties of Pinus sylvestris timber, which had been equilibrated to a moisture content of 12%. Mechanical characterization followed standardized protocols: bulk density was determined as 0.493 g/cm³ according to GB/T 1933-2009, while elastic constants (including Young's moduli E, Poisson's ratios v, and shear moduli G) were acquired using resistance-based strain measurements compliant with GB/T 15777-2017, GB/T 1943-2009, and LY/T 3297-2022 standards. Material strength evaluation indicated 35.2 MPa in longitudinal compression (GB/T 1935-2009), 5.14 MPa under transverse compression (GB/T 1939-2009), and a flexural strength of 52.9 MPa (GB/T 1936.1-2009). These standards specify the full testing procedures, including specimen preparation, loading conditions, and data processing, to systematically determine the density, elastic constants, and strength parameters of the wood. Constitutive parameters were calibrated iteratively against empirical test data. Plasticity was represented using Hill's anisotropic yield criterion, while elastic response was captured through an orthotropic constitutive formulation consistent with established approaches (Yao and Li 2023). The model incorporated nine independent constants to define orthotropy, comprising three Young's moduli (E_1, E_2, E_3) , three shear moduli (G_{12}, G_{13}, G_{23}) , and three Poisson's ratios (v_{12} , v_{13} , v_{23}). The finite element model incorporated the following simplifying assumptions: First, the wood material was modeled as an orthotropic and defect-free continuum; Second, frictional effects at component interfaces were neglected;

Third, all structural components were assumed to be perfectly bonded at mortise-tenon joints; Fourth, symmetry in geometry and material properties was maintained throughout the model.

Loading Protocol

The loading protocol followed the coordinate system illustrated in Fig. 5. Monotonic static forces (Chen *et al.* 2014) were applied vertically in the Z-direction to simulate sustained roof loads. In the horizontal plane, bidirectional low-cycle reversed displacements (Meng *et al.* 2018; Wang *et al.* 2025) were introduced along the Y- and X-axes to represent seismic effects.

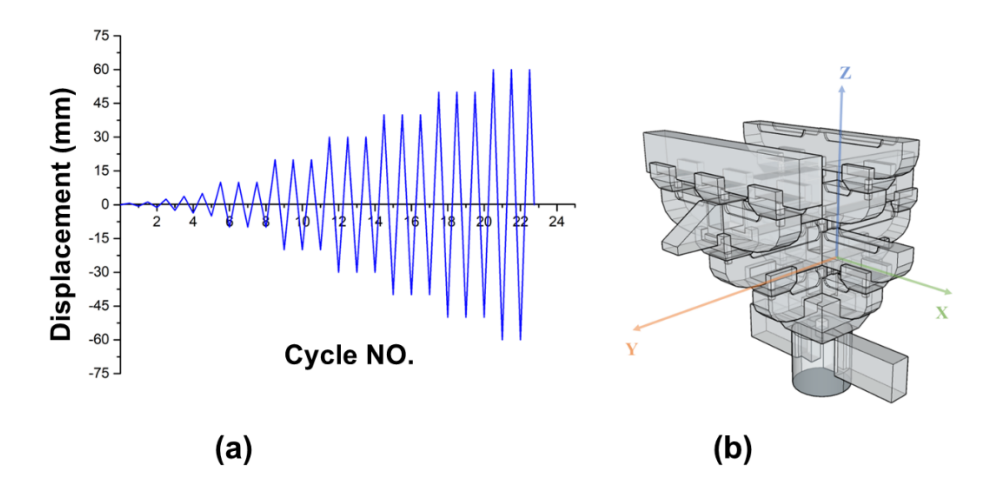


Fig. 5. Definition of the loading protocol (a) and coordinate system (b) for the experimental model

Vertical monotonic static tests were carried out following the procedure established by Niu (2017), aiming to replicate the load-transfer behavior of permanent roof loads in traditional Chinese Dougong structures. An initial vertical load of 60 kN was introduced, which reflected the estimated roof load derived from architectural standards and structural calculations. A hybrid loading strategy combining force and displacement control was implemented in two successive stages. Initially, force-controlled loading was applied at a steady rate of 5 kN/min until the specimen yielded, as indicated by visible deformations or marked nonlinearity in the load–displacement curve. The test then transitioned to displacement control at a rate of 2 mm/min to investigate post-yielding performance. The stopping conditions in this phase were set as either structural collapse—operationally defined as a drop in load-bearing capacity to 80% of the maximum resistance—or extensive damage preventing further loading. This two-stage approach allowed for a detailed characterization of both elastic and plastic response, while maintaining controlled monitoring throughout the failure progression.

A quasi-static cyclic test was performed under horizontal low-frequency reversed loading following a displacement-controlled procedure (Yao and Li 2023). The loading protocol consisted of two main stages: the initial stage involved five monotonic cycles with stepwise increased amplitudes $(0.0125\Delta, 0.025\Delta, 0.05\Delta, 0.075\Delta,$ and 0.1Δ , where $\Delta = 50$ mm). In the subsequent stage, three full cycles were applied at each amplitude level, beginning at 0.2Δ and increasing incrementally by 0.2Δ per step (Cao *et al.* 2021). A schematic of the loading protocol is provided in Fig. 5a. Numerical simulations were

configured such that solver settings, interfacial interactions, and boundary conditions were consistently aligned with the experimental setup along the Z-, Y-, and X-axes, as depicted in Fig. 5b.

Grid System

The finite element model was developed using second-order elements and a hybrid meshing approach combining hexahedral and tetrahedral elements. Hexahedral meshes were used to discretize regions with regular geometry, whereas tetrahedral elements were employed for more complex architectural features. The resulting mesh configuration of the Dougong bracket assembly is illustrated in Fig. 6.

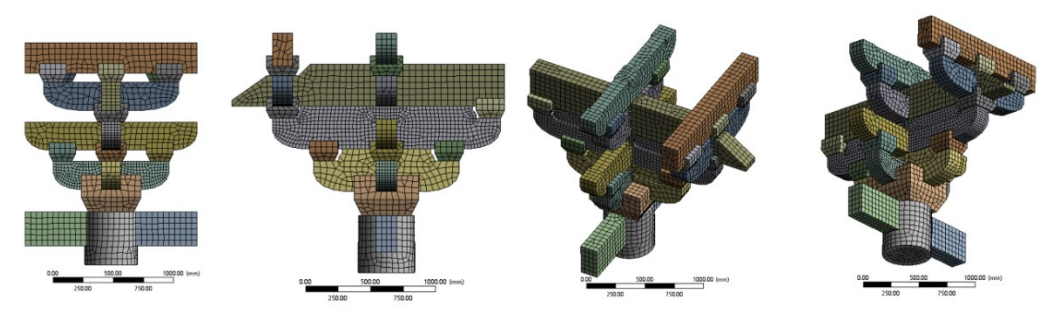


Fig. 6. Division of Dougong bracket's grid system in simulation

RESULTS AND DISCUSSION

Monotonic Vertical Loading (Z-axis)

Figure 7 presents the load-displacement curve derived from the vertical monotonic loading simulation along the Z-axis. The simulated bearing capacity of the Dougong bracket model showed no convergence beyond 344 kN. Under Z-axis loading, the Von Mises stress distribution (Fig. 8A) was primarily concentrated in the upper structural elements aligned with the loading path. A peak stress value of 27.4 MPa was identified at the *Huagong/Ludou* interface, coinciding with the central mortise-tenon joint. A similar distribution pattern was observed for the elastic strain (Fig. 8B), where the maximum strain value reached 0.0427 at the same critical interface. The strain energy density distribution (Fig. 8C) exhibited spatial agreement with the stress concentrations, reaching 53,000 MJ at the *Ludou*/column-head junction. This localized energy accumulation corroborates the efficient transfer of load from upper components to the supporting columns within the Dougong system. Displacement analysis (Fig. 8D) indicated a gradually decreasing deformation gradient, declining from 174 mm at the *Liaoyanfang* top relative to the fixed support at the column base, which aligns with the hierarchical deformation pattern typical of traditional timber structures under vertical loads.

While the present results clearly delineate the static and cyclic behavior of this specific Dougong, their significance is further illuminated when contrasted with the mechanical responses documented in other historic timber joint systems, such as those found in Japanese temple construction or European medieval timber frames, as explored in prior literature (Fujita *et al.* 2001).

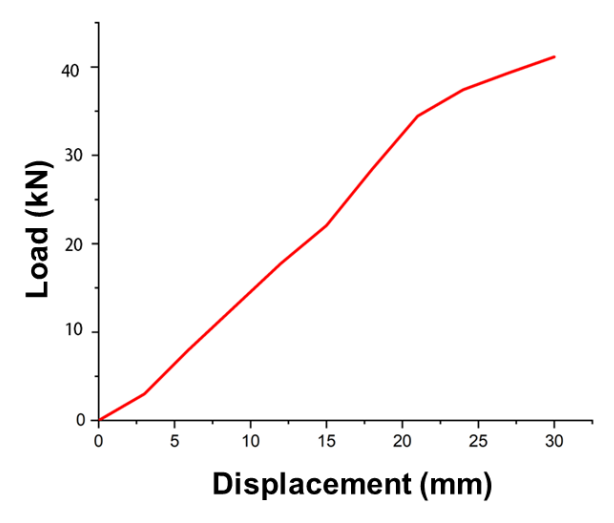


Fig. 7. The load-displacement curve in Z-axis

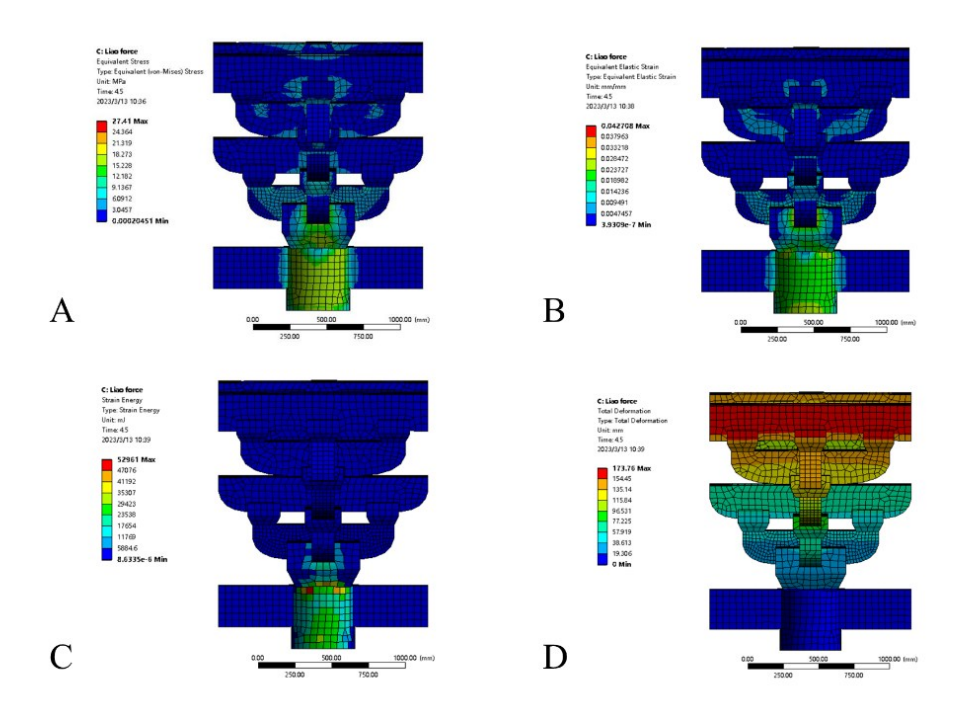


Fig. 8. The Von Mises stress distribution (A), Strain (B), Strain energy density (C), and Displacement (D) under Z-Axis loading

Bidirectional Low-Cycle Reversed Cyclic Loading (Y- and X-Axes)

Figure 9 displays the simulation outcomes from the horizontal low-frequency bidirectional cyclic loading tests conducted along the Y- and X-axis directions, illustrating the hysteretic load-displacement behavior of the Dougong bracket. The tested model reached a maximum lateral load of 999 kN along the Y-axis and 522 kN along the X-axis. The hysteresis loops for both directions exhibit symmetric, spindle-shaped forms with a tendency toward rectangularity, reflecting significant energy dissipation, stable plastic deformation capacity under repeated cyclic loading, and the influence of the mortise-tenon joints' frictional slip and re-engagement behavior.

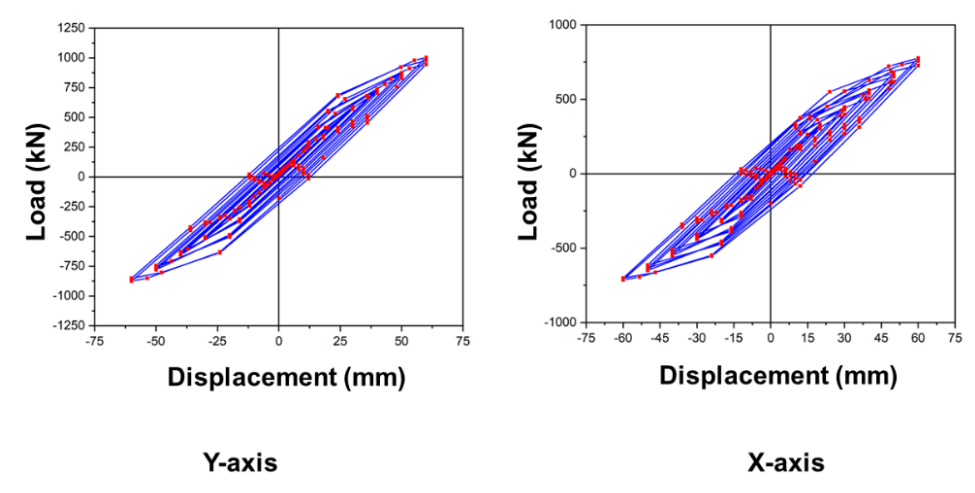


Fig. 9. Hysteresis Loops under Y- and X-Axis Loading

Based on the hysteretic response, the skeleton curve representing the load-displacement relationship was derived, as shown in Fig. 10. Furthermore, the stiffness degradation behavior of the specimen was quantified by calculating the secant stiffness at key points along the skeleton curve, with the resulting degradation profile presented in Fig. 11.

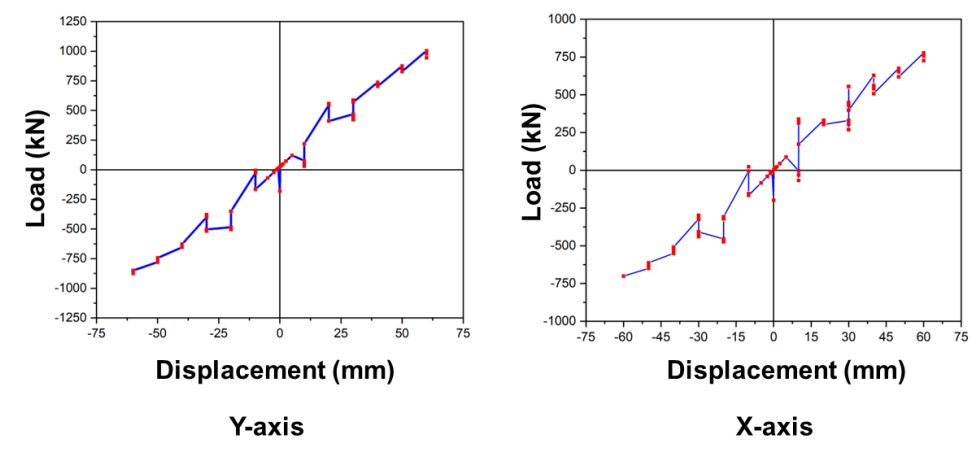


Fig. 10. Skeletal curves under Y- and X-axis loading

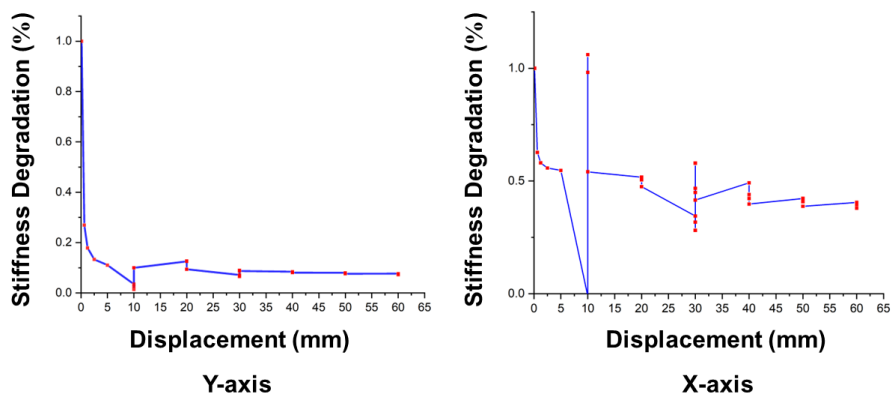


Fig. 11. Stiffness degradation under Y- and X-axis loading

As shown in Fig. 12A, the Von Mises stress distribution revealed significant stress concentrations, mainly occurring at the *Huagong*-to-column-head interface. A maximum stress value of 30.5 MPa was observed at the connection between the upper-layer *Huagong* and *San Dou*. A similar spatial distribution was evident in the elastic strain field (Fig. 12B), where the peak strain reached 0.0372, also located at the same *Huagong–San Dou* junction. The strain energy density distribution (Fig. 12C) corresponded closely with the stress concentrations, illustrating efficient energy transmission through the arch-rafter-bucket structural assembly down to the columns. The highest strain energy accumulation, measured at 2.34×10⁶ MJ, was identified at the *Huagong–San Dou* interface, marking it as the critical zone for energy dissipation. Displacement outcomes (Fig. 12D) indicated a graded deformation profile, with the maximum displacement of 10.1 mm appearing again at the *Huagong–San Dou* joint, followed by progressively smaller deformations throughout the *Liaoyanfang*, *Linggong*, *Ludou*, and column-head regions.

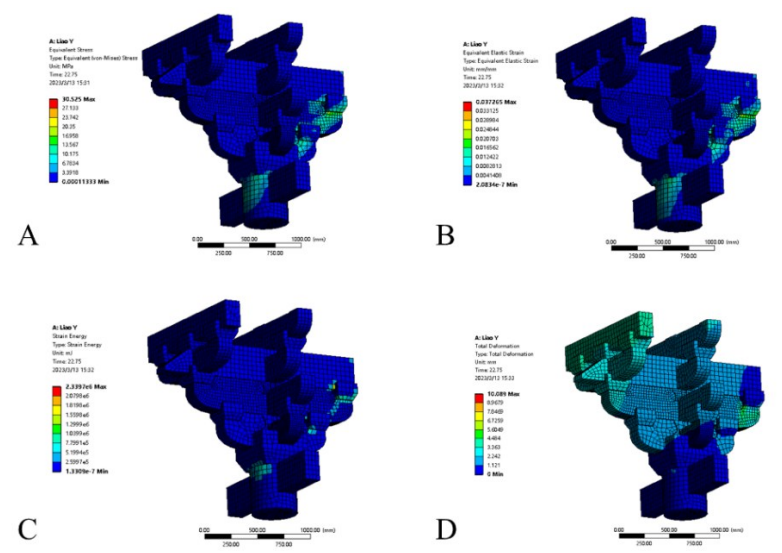


Fig. 12. Analysis of Y-Directional, Von Mises Stress (A), Equivalent Elastic Strain (B), Strain Energy Density Fields (C), and Displacement (D)

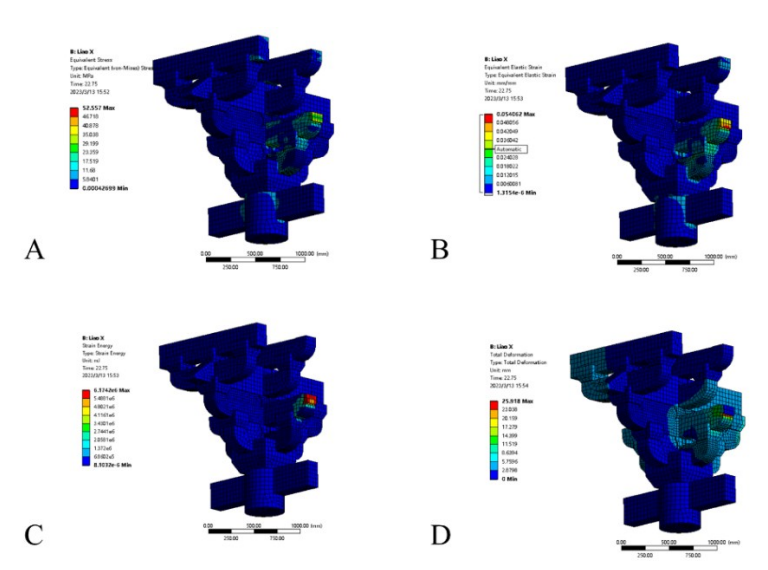


Fig. 13. Analysis of X-Directional, Von Mises Stress (A), Equivalent Elastic Strain (B), Strain Energy Density Fields (C), and Displacement (D)

Under quasi-static loading conditions applied along the X-axis, the Von Mises stress field (Fig. 13A) exhibited significant concentrations in several critical regions. These included the mortise-tenon joint connecting the right *Mangong* and *Nidaogong*, as well as the interface between the right side of the *Nidaogong* and the column-head. The maximum stress value observed in these regions reached 52.6 MPa. This pattern of stress localization aligned closely with the distribution of equivalent elastic strain (Fig. 13B), where the highest strain value, 0.054, was identified at the right side of the *Mangong*. The spatial consistency between these two fields confirms that areas of high stress correspond directly to regions of elevated strain.

The distribution of strain energy density (Fig. 13C) exhibited a pattern consistent with stress concentration, with a maximum value of 6.17×10^6 MJ observed on the right side of the *Mangong* component. This localization of energy implies that the mortise-tenon joint serves as a critical region for energy dissipation under cyclic loading conditions. Analysis of displacement (Fig. 13D) indicated that the maximum deformation, reaching 25.9 mm, also occurred on the right side of the *Mangong*. The structural deformation gradient diminished progressively toward the foundation, a response that aligns with typical deformation mechanisms of traditional timber structures under lateral loads. Furthermore, the integrated analysis of stress, strain, and energy revealed that the interface between the *Mangong* and *San Dou* represents a potential initiation point for failure, where both mechanical stress and strain energy density surpass critical thresholds documented in comparable timber joint configurations. This proposed failure mechanism is consistent with documented damage patterns in historical timber structures experiencing cyclic lateral loading.

Modeling the Static Behavior of Structures (Z-axis, Y-axis, and X-axis)

Under monotonic loading along the Z-axis, the five-tiered outer eave column-head Dougong specimen displayed a three-stage elastic stiffness degradation pattern (Fig. 14), with each phase reflecting distinct mechanical behaviors. Phase OA (0-- Δ A) was associated with the closure of initial gaps and possible loose fits at mortise-tenon joints, leading to contact-induced nonlinearity and a relatively low structural stiffness of 1.25 kN/mm, as computed using Eq. 1. Subsequently, Phase AB (Δ A- Δ B) exhibited linear elastic response with a stabilized stiffness value of 3.61 kN/mm (derived from Eq. 2), indicating full engagement and interaction among the constituent elements. Finally, Phase BC (Δ B- Δ C) was governed by a progressive reduction in stiffness, which decreased to 2.48 kN/mm in accordance with Eq. 3, primarily due to yielding within the mortise-tenon joints and the accumulation of structural damage.

$$k_{OA} = \frac{P_X}{\Delta_Y} \tag{1}$$

$$k_{AB} = \frac{P_{y} - P_{x}}{\Delta_{y} - \Delta_{x}} \tag{2}$$

$$k_{BC} = \frac{P_b - P_y}{\Delta_b - \Delta_y} \tag{3}$$

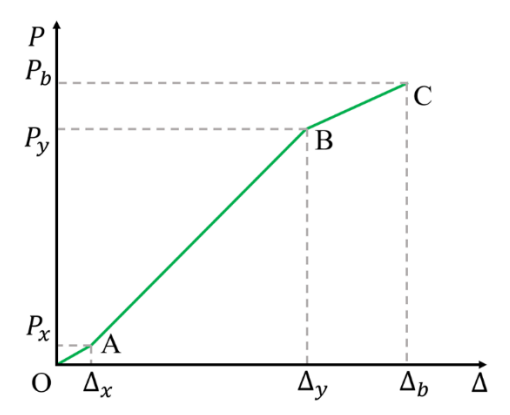


Fig. 14. Triphasic elastic stiffness degradation of the specimen under monotonic Z-axis loading

Based on the analyzed hysteresis behavior and skeleton curves, a restoring force model (Fig. 15) was developed to characterize the quasi-static structural response of the five-tiered outer eave column-head Dougong test specimen under bidirectional loading along the Y- and X-axes.

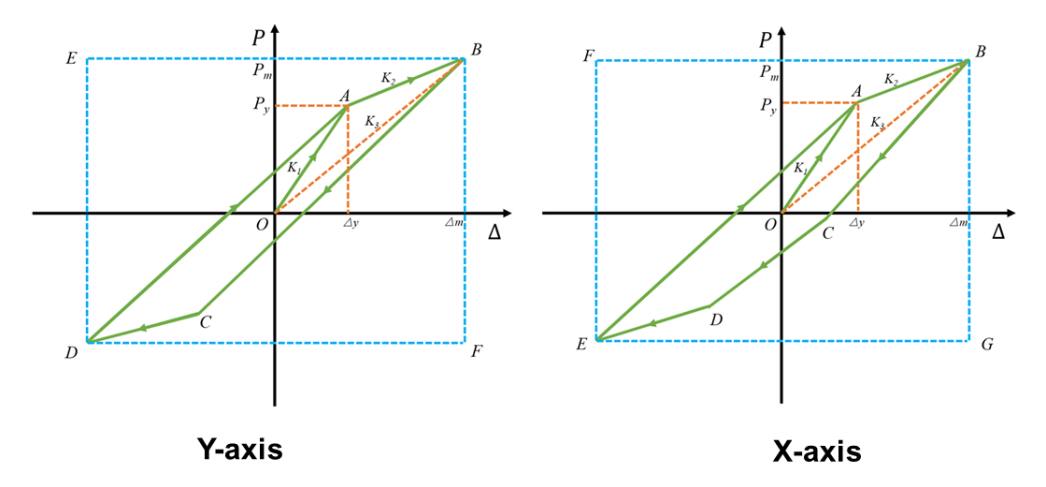


Fig. 15. Hysteresis model of the structural system under quasi-static X- and Y-directional loading

Under monotonic Y-axis loading, the mechanical response of the test specimen exhibited three distinct deformation phases. The initial segment OA represented the elastic stage, during which the displacement increased linearly with the applied load, yielding an initial stiffness K_{Y1} of 29.98 kN/mm. Subsequent segment AB corresponded to the yield phase, where a marked reduction in stiffness was observed; the calculated stiffness K_{Y2} in this plastic regime was 6.95 kN/mm. The effective stiffness, denoted as K_{Y3} and defined as the ratio of the maximum load-bearing capacity to the peak displacement in the restoring force model, was determined to be 17.1 kN/mm. An analogous mechanical behavior was identified under X-axis loading, characterized by an elastic stiffness K_{X1} of 33.3 kN/mm, a plastic stiffness K_{X2} of 5.66 kN/mm, and an effective stiffness K_{X3} of 12.4 kN/mm.

When the Dougong bracket is conceptualized as a damping element between the roof and column in traditional Chinese timber structures, the nonlinear coefficient *NL* can be introduced to quantitatively assess its energy dissipation performance. The *NL* is defined as the ratio of the envelope area of the restoring force model to the rectangular area SBDEF, as illustrated in Fig. 15. This coefficient serves as an indicator of the energy absorption

capability of the Dougong component. For the five-tiered outer eave column-head Dougong test model, the measured *NL* values were 0.173 along the Y-axis direction and 0.203 along the X-axis direction.

The ductility of the Dougong bracket, defined as the ratio of its ultimate displacement to yield displacement, reflects the component's deformation capacity, with a higher value indicating superior deformability. According to the simulation results, the ductility of the five-tiered outer eave column-head Dougong test model was 2.45 in the Y-axis direction and 3.63 in the X-axis direction.

The energy dissipation capacity of the Dougong bracket component was found to be positively correlated with its equivalent viscous damping coefficient (h_e), where a larger value indicates stronger damping performance. This coefficient was calculated based on the methodology outlined in Fig. 16 and Eq. 4. For the five-tiered outer eave column-head Dougong bracket test model, the equivalent viscous damping coefficient is 0.097 in the Y-axis direction and 0.122 in the X-axis direction.

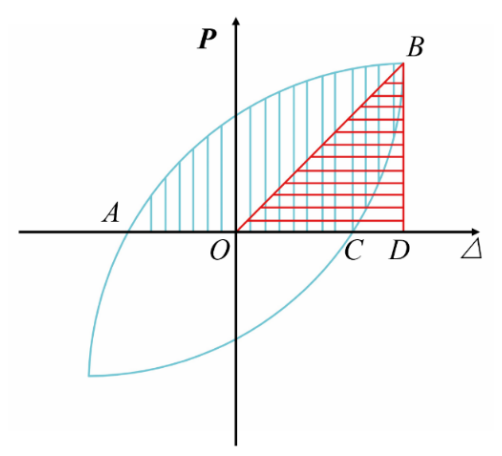


Fig. 16. Calculation of equivalent viscous damping coefficient

$$h_e = \frac{1}{2\pi} \cdot \frac{S_{ABC}}{S_{OBD}} \tag{4}$$

The static structural performance and stress-deformation behavior of a full-scale Five-tier Outer Eave Column-head Dougong Bracket test model, based on the Liao Dynasty Dule Temple Gate, were investigated through three-dimensional analysis (X-, Yand Z- axes). Under monotonic vertical static loading in the Z-direction, the structural response followed a variable-stiffness elastic model, which evolved through three distinct mechanical phases: Phase I involved the compaction of gaps and interfaces between components; Phase II was marked by linear elastic behavior with nearly constant stiffness; and Phase III concluded with yield initiation and ultimate failure. Under low-cycle reversed horizontal loading along the Y- and X-axes, the response adheres to a multi-linear restoring force model, advancing sequentially through elastic, yielding, and failure stages. The loading process exhibited progressive stiffness degradation across the Dougong assembly. Observed hysteresis loops demonstrate pinching near the origin, suggesting interfacial slip mechanisms. Beyond the critical load level, significant plastic deformation developed, accompanied by a rapid increase in displacement. Key mechanical properties—including strength, deformation capacity, and energy dissipation efficiency—evaluated along all three axes, are comprehensively summarized in Table 1. Experimental findings indicate that structural damage initiates at critical nodal regions under overload conditions, followed by force redistribution that ultimately leads to progressive collapse of the system.

Table 1. Key Parameters of the Six Experimental Assemblies

| Name | Five-tier Outer Eave Column-head Dougong Bracket | | | | | |
|-----------------|--|-----------------|-----------------|-----------------|--------------------|--|
| | from the Liao Dynasty Dule Temple Gate | | | | | |
| Pathway | Modeling and Simulation | | | | | |
| Strength | | Deformation | | | Energy Dissipation | |
| F _{Z1} | F _{Z2} | K _{Z1} | K _{Z2} | K _{Z3} | NL(Y) | |
| 306.81 | 343.52 | 1.25 | 3.61 | 2.48 | 0.173 | |
| F _{Y1} | F _{Y2} | K _{Y1} | K _{Y2} | K _{Y3} | NL(X) | |
| 998.57 | 998.57 | 29.98 | 6.95 | 17.09 | 0.203 | |
| F _{X1} | F _{X2} | K _{X1} | K _{X2} | Кхз | H _Y | |
| 521.56 | 521.56 | 33.34 | 5.66 | 12.43 | 0.097 | |
| | | U _Y | Ux | | Hx | |
| | | 2.45 | 3.63 | | 0.122 | |

^{*} F_{Z1} and F_{Z2} denote the yield and ultimate bearing capacities (in kN), respectively, under Z-axis loading. Similarly, F_{Y1} and F_{Y2} indicate the maximum positive and negative horizontal thrusts (in kN) along the Y-axis, while F_{X1} and F_{X2} represent those along the X-axis. In terms of stiffness parameters under Z-axis loading, K_{Z1} corresponds to the initial stiffness, K_{Z2} to the yield stiffness, and K_{Z3} to the ultimate stiffness (all in kN/mm). For Y-axis loading, K_{Y1} , K_{Y2} , and K_{Y3} refer to the elastic, plastic, and effective stiffnesses (in kN/mm), respectively. Likewise, K_{X1} , K_{X2} , and K_{X3} describe the elastic, plastic, and effective stiffnesses (in kN/mm) under X-axis loading. The ductility values along the Y and X axes are represented by U_Y and U_X , respectively. Nonlinear coefficients in the Y- and X-axis directions are designated as NL(Y) and NL(X), while H_Y and H_X correspond to the equivalent viscous damping coefficients along the respective axes.

CONCLUSIONS

- 1. The static structural response of the 'Five-tier Outer Eave Column-head Dougong Bracket' test model, based on the Liao Dynasty Dule Temple Gate, under vertical monotonic loading along the Z-axis was characterized by a variable-stiffness linear elastic mechanical model. Conversely, under low-cycle reversed quasi-static loading along the Y- and X-axes, the behavior can be accurately represented using a restoring force model.
- 2. In terms of strength, the Dougong bracket test model from the Liao Dynasty exhibited a yield bearing capacity of 307 kN and an ultimate bearing capacity of 344 kN under Z-axis loading. Under horizontal loading, the maximum thrust reached 999 kN along the Y-axis and 522 kN in the positive X-axis direction.
- 3. In terms of deformation performance, the Liao Dynasty Dougong bracket test model exhibited the following mechanical properties: under Z-axis loading, the initial stiffness was 1.25 kN/mm, the yield stiffness 3.61 kN/mm, and the deformation stiffness 2.48 kN/mm. Along the Y-axis, the elastic, plastic, and effective stiffness values were 29.98 kN/mm, 6.95 kN/mm, and 17.09 kN/mm, respectively, with a ductility of 2.45. Similarly, the X-axis direction showed elastic, plastic, and effective stiffness values of 33.3 kN/mm, 5.66 kN/mm, and 12.43 kN/mm, respectively, accompanied by a ductility of 3.63.

- 4. In terms of energy dissipation characteristics, the Liao Dynasty Dougong bracket test model exhibited a nonlinear coefficient of 0.173 and an equivalent viscous damping coefficient of 0.097 along the Y-axis; the corresponding values along the X-axis were 0.203 and 0.122, respectively.
- 5. The findings offer a foundational understanding for assessing similar historic structures. Future research should focus on experimental validation and developing guidelines for applying these results in the rehabilitation of real-world conservation projects. This numerical study provides reliable predictions of the Dougong bracket's mechanical behavior, laying a foundation for future experimental validation through physical testing.

ACKNOWLEDGMENTS

This work was supported by the Fundamental Research Funds for Inner Mongolia University of Science & Technology (Grant No. 2024QNJS023) and the Scientific Research Projects of First-class Disciplines (Grant No. YLXKZX-NKD-027).

The authors used DeepSeek artificial intelligence to polish the text. The images, numbers, graphics, or diagrams in this article are not produced using any generative AI.

REFERENCES CITED

- Chen, Z., Zhu, E., Lam, F., and Pan, J. (2014). "Structural performance of Dou-Gong brackets of Yingxian Wood Pagoda under vertical load-An experimental study," *Engineering Structures* 80, 274-288. https://doi.org/10.1016/j.engstruct.2014.09.013
- Chen, J., Chen, Y. F., Shi, X., Zhao, Y., and Li, T. (2018). "Hysteresis behavior of traditional timber structures by full-scale tests," *Advances in Structural Engineering* 21(2), 287-299. https://doi.org/10.1177/1369433217717117
- Chen, C., Li, Y., Han, D., Kang, H., and Li, Y. (2025). "Simulation study on the static characteristics of 'Five-tier Outer Eave Column-head Dougong Bracket' from the main hall of Nanchan Temple in Tang Dynasty," *BioResources* 20(3), 6082-6099. https://doi.org/10.15376/biores.20.3.6082-6099
- Deng, Y., Li, Y., and Li, A. (2023). "Seismic safety assessments of historical timber buildings using updated finite element models: Case study of Yingxian wooden pagoda, China," *Journal of Building Engineering* 63, article 105454. https://doi.org/10.1016/j.jobe.2022.105454
- Fujita, K., Kimura, M., Ohashi, Y., and Sakamoto, I. (2001). "Hysteresis model and stiffness evaluation of bracket complexes used in traditional timber structures based on static lateral loading tests," *Journal of Structural and Construction Engineering* 66(543), 121-127. https://doi.org/10.3130/aijs.66.121 2
- GB/T 1933 (2009). "Method for determination of the density of wood," Standardization Administration of China, Beijing, China.
- GB/T 1935 (2009). "Method of testing in compressive strength parallel to grain of wood," Standardization Administration of China, Beijing, China.
- GB/T 1936.1 (2009). "Method of testing in bending strength of wood," Standardization Administration of China, Beijing, China.

- GB/T 1939 (2009). "Method of testing in compression perpendicular to grain of wood," Standardization Administration of China, Beijing, China.
- GB/T 1943 (2009). "Method for determination of the modulus of elasticity in compression perpendicular to grain of wood," Standardization Administration of China, Beijing, China.
- GB/T 15777 (2017). "Method for determination of the modulus of elasticity in compression parallel to grain of wood," Standardization Administration of China, Beijing, China.
- Liu, P., Yeo, S.Y., and Fukuda, H. (2025). "Unraveling the vertical compressive performance of Dou in Chinese architectural heritage: Impact of grain direction and timber species," *Structures* 77, article 109126. https://doi.org/10.1016/j.istruc.2025.109126
- LY/T 3297 (2022). "Dynamic test method for shear modulus of wood," Standardization Administration of China, Beijing, China.
- Meng, X., Li, T., Yang, Q., and Wei, J. (2018). "Seismic mechanism analysis of a traditional Chinese timber structure based on quasi-static tests," *Structural Control Health Monitoring* 25(10), article e2245. https://doi.org/10.1002/stc.2245
- Meng, X., Yang, Q., Wei, J., and Li, T. (2018). "Experimental investigation on the lateral structural performance of a traditional Chinese pre-Ming dynasty timber structure based on half-scale pseudo-static tests," *Engineering Structures* 167, 582-591. https://doi.org/10.1016/j.engstruct.2018.04.077
- Meng, X., Li, T., and Yang, Q. (2019). "Experimental study on the seismic mechanism of a full-scale traditional Chinese timber structure," *Engineering Structures* 180, 484-493. https://doi.org/10.1016/j.engstruct.2018.11.055
- Niu, Q. (2017). Experimental Study and Theoretical Analysis on Half-Scale Model of Timber Structure in Song Dynasty, Master's Thesis, Taiyuan University of Technology, Taiyuan, China.
- Song, D., Xue, J., and Xu, C. (2023). "Hysteretic behaviors of Pingshenke Dou-Gong brackets of ancient timber buildings under different loading directions," *Structures* 51, 1944-1958. https://doi.org/10.1016/j.istruc.2023.03.164
- Sciomenta, M., Bedon, C., Fragiacomo, M., and Luongo, A. (2018). "Shear performance assessment of timber log-house walls under in-plane lateral loads via numerical and analytical modelling," *Buildings* 8(8), article 99. https://doi.org/10.3390/buildings8080099
- Sha, B., Xie, L., Yong, X., and Li, A. (2021). "An experimental study of the combined hysteretic behavior of dougong and upper frame in Yingxian Wood Pagoda," *Construction and Building Materials* 305, article 124723. https://doi.org/10.1016/j.conbuildmat.2021.124723
- Sha, B., Li, A., Deng, Y., and Xie, L. (2024). "Study on the damage mechanism and hysteretic performance of fork column-dougong connection in traditional Chinese multi-story wooden structures," *Journal of Building Engineering* 84, article 108502. https://doi.org/10.1016/j.jobe.2024.108502
- Wang, J., Tu, C., Chen, Z., and Wang, X. (2025). "Experimental study on the mechanical behavior and degradation law of Tang dynasty palace-style single-room timber frame," *Structures* 73, article 108469. https://doi.org/10.1016/j.istruc.2025.108469
- Wu, Y., Song, X., Gu, X., and Luo, L. (2018). "Dynamic performance of a multi-story traditional timber pagoda," *Engineering Structures* 159, 277-285. https://doi.org/10.1016/j.engstruct.2018.01.003

- Wu, Y., Song, X., Ventura, C., and Lam, F. (2020). "Modeling hysteretic behavior of lateral load-resisting elements in traditional Chinese timber structures," *Journal of Structural Engineering* 146(5), article 04020062. https://doi.org/10.1061/(ASCE)ST.1943-541X.0002613
- Wang, J., Cui, Z., Yu, L., Xu, R., and Yang, Q. (2022). "Analysis of the seismic behavior of traditional Chinese timber structures in the Tang Dynasty," *Structures* 41, 447-462. https://doi.org/10.1016/j.istruc.2022.05.007
- Xue, J. Y., Wu, Z. J., Zhang, F. L., and Zhao, H. T. (2016). "Seismic damage evaluation model of Chinese ancient timber buildings," *Advances in Structural Engineering* 18(10), 1671-1683. https://doi.org/10.1260/1369-4332.18.10.1671
- Yao, L. and Li, Y. (2023). "Simulation study on static characteristics of Qing-style 'One Bucket Three Liters' column-cap Dou-Gong bracket," *BioResources* 18(4), 6955-6970. https://doi.org/10.15376/biores.18.4.6955-6970

Article submitted: September 1, 2025; Peer review completed: November 5, 2025; Revised version received: November 8, 2025; Accepted: November 9, 2025; Published: November 14, 2025.

DOI: 10.15376/biores.21.1.221-236